Determination of Charge-Carrier Mobility and Built-In Potential in Thin-Film Organic *M-I-M* Diodes from Extraction-Current Transients

Staffan Dahlström,* Oskar J. Sandberg, Mathias Nyman, and Ronald Österbacka

Physics, Faculty of Science and Engineering and Center for Functional Materials, Åbo Akademi University, Porthansgatan 3, 20500 Turku, Finland

(Received 19 December 2017; revised manuscript received 4 September 2018; published 8 November 2018)

We have extended the Charge Extraction by a Linearly Increasing Voltage (CELIV) technique for determination of the built-in potential and the charge-carrier mobility in thin-film metal-insulator-metal (*M-I-M*) diodes. The validity of the presented analytical theory is verified by drift-diffusion simulations and experimentally demonstrated on organic solar cells. In contrast to the original CELIV theory, which assumes a uniform charge-carrier distribution in the active layer of the device, here we derive an analytical expression for determining the built-in potential and mobility in the case of a nonuniform charge-carrier distribution where charges have diffused into the active layer from the contacts. The extended CELIV theory is applicable on all thin-film *M-I-M* diodes, e.g., organic solar cells. Drift-diffusion simulations show that the error for mobility estimation can be an order of magnitude if not correcting for the carrier profile.

DOI: 10.1103/PhysRevApplied.10.054019

I. INTRODUCTION

Organic semiconductors are of great interest in the fields of optoelectronics and thermoelectrics due to their suitability for low-cost and large-area applications. In order to improve the performance of devices based on these materials, it is essential to have reliable characterization techniques for determining parameters relevant for the device physics, such as the charge-carrier mobility and built-in potential. One commonly used method for determining the charge carrier mobility is the Charge Extraction by a Linearly Increasing Voltage (CELIV) technique [1]. The advantage of CELIV, in addition to its simplicity and modest equipment requirement, is that it can be used on operating devices, for example, thin-film solar cells. However, the original CELIV theory is derived for a doped device with blocking contacts, which severely limits the applicability of the method. In order to be able to use CELIV on any metal-insulator-metal (*M-I-M*)-type diode, which constitutes a majority of present day thin-film solar cells, the theory needs to be revised.

The CELIV technique is based on applying a linearly increasing voltage pulse in reverse bias of the device for equilibrium charge-carrier extraction. In dark, the measured extracted charges can originate either from: i) diffusion or injection from the contacts or ii) doping of the active layer. A schematic picture of the CELIV method is shown in Figs. 1(a) and 1(b). The charge-carrier mobility μ can be calculated from the time the measured current transient reaches its maximum $t_{\max}$ using

$$\mu = K\frac{2d^2}{3At_{\max}^2}, \tag{1}$$

where d is the active layer thickness, A is the slope of the linearly increasing voltage pulse, and K is a correction factor. Equation (1) is based on the original CELIV theory by Juška *et al.* [1], assuming a uniform distribution of charge carriers of low concentration (negligible space-charge effects) in the active layer, corresponding to $K = 1$. At higher concentrations, the impact of the electric field redistribution is taken into account by introducing a correction factor $K \neq 1$. Juška *et al.* [2] originally presented $K = [1 + 0.36\Delta j\,(t_{\max})/j_0\,]^{-1}$, where j_0 is the geometric capacitive response and $\Delta j\,(t_{\max})$ is the maximum of the time-dependent extraction current, however, alternative correction factors, providing slightly better numerical approximations within the moderate conductivity regime [$\Delta j\,(t_{\max}) \sim j_0$], have been suggested in the literature [3–5]. Lorrmann *et al*. provide the best approximation [5] and it is used in this paper.

The mobility determination using the standard CELIV theory, Eq. (1), is generally not valid in organic thin-film devices, due to extraction of pre-existing nonuniform carrier profiles [6–8]. For example, Hanfland *et al*. [9] found that even at a low amount of trapping (trap depths smaller than kT/e), the mobility obtained by Eq. (1) of undoped organic solar cells in the dark deviated by an order of magnitude from the actual one over a wide range of mobilities. This type of undoped device with nonblocking contacts typically exhibit highly nonuniform charge-carrier

*stdahlst@abo.fi

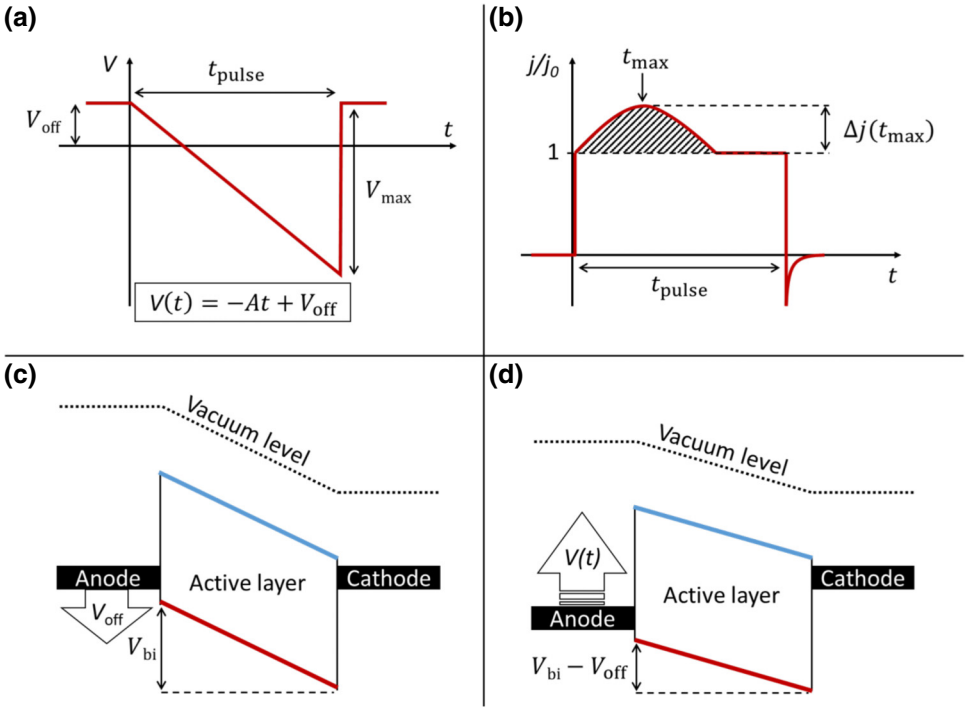

FIG. 1. The linearly increasing voltage pulse $V(t) = -At + V_{off}$ applied in a CELIV measurement is plotted in (a). In (b), a schematic of the corresponding current transient response consisting of a geometric capacitive part j_0 and a time-dependent extraction current $\Delta j(t)$ is shown. In (c) and (d), a schematic of the band diagram in a *M-I-M* diode is shown, where (c) illustrates how diffusion of charge-carriers into the active layer is assisted by a small steady-state offset voltage V_{off}, applied in forward bias, and (d) shows how charge carriers are extracted by a linearly increasing voltage pulse applied in reverse bias.

distributions due to diffusion of charge carriers from the contacts. For an accurate determination of the mobility from CELIV measurements on thin-film devices, it is, therefore, essential to take the carrier distribution within the semiconductor layer into account.

In this paper, we extend the CELIV theory to thin-film *M-I-M* diodes with injecting contacts by taking into account the effects of diffusion and a built-in potential on the transient currents. The extended method allows for simultaneous determination of the built-in potential and the charge-carrier mobility. The presented analytical theory is verified by drift-diffusion simulations of extraction-current transients and is experimentally demonstrated on organic solar cell devices.

II. THEORY

The device under consideration is an organic *M-I-M* diode, where the active layer consists of an intrinsic (undoped) organic semiconductor layer, sandwiched between a hole-injecting anode (at $x = 0$) and an electron-injecting cathode (at $x = d$). The built-in potential over the device is given by V_{bi}. A linearly increasing voltage pulse $V(t) = -At + V_{off}$ is applied over the device, where V_{off} is a small steady-state offset voltage and $A = V_{max}/t_{pulse}$ is given by the maximum transient voltage applied V_{max}, divided by the length of the voltage pulse t_{pulse}. The linear voltage pulse is applied in reverse bias in order to prevent current injection during the extraction process. The steady-state offset voltage is applied in forward bias in order to increase the number of dark charge carriers to extract. A schematic of the applied voltage pulse, current transient, and the corresponding energy-level diagrams are shown in Fig. 1. Note that the measurements are performed in the dark, meaning that each charge-carrier type is injected from its respective contact. This is different from using a light pulse for generating free charge carriers, as in the photo-CELIV technique, where both electrons and holes are generated at the same position in the active layer according to the light absorption profile.

At small offset voltages, $0 \leq V_{off} < V_{bi}$, the charge-carrier profiles decrease exponentially from the injecting contacts [10–12], whereas the electric field prior to the application of the pulse at $t = 0$ is given by $F_0 = (V_{off} - V_{bi})/d \equiv -U/d$. To simplify the analysis, in the following we assume the current transport to be hole-dominated (the spatially averaged hole conductivity is much larger than that of electrons). In this case, μ is the hole mobility. An analogous treatment is valid for electron-dominated transport. The dark hole current flowing through the device under steady-state conditions can be expressed as $J_{off} = e\mu F_0 p_0(x) - \mu kT dp_0/dx$ with the hole density, prior to the pulse, then given by

$$p_0(x) = \frac{(N_1 - N_2)\exp(eF_0x/kT) - N_1\exp(eF_0d/kT) + N_2}{1 - \exp(eF_0d/kT)} \approx N_1 \exp\left(-\frac{eUx}{kTd}\right) \quad (2)$$

where $eU \gg kT$ and $N_1 \gg N_2$ are assumed in the last step; N_1 and N_2 are the hole densities at the anode and cathode,

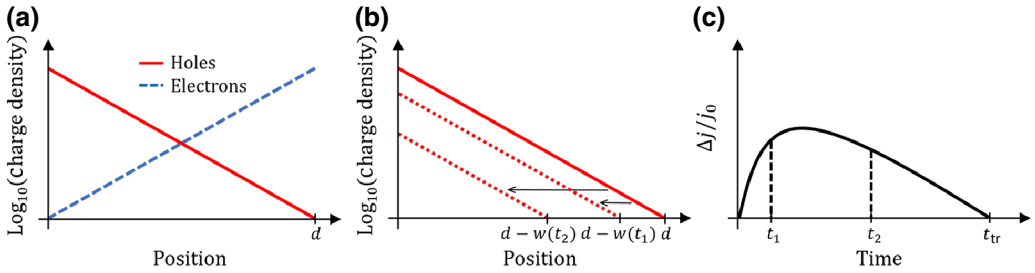

FIG. 2. The exponential distribution of equilibrium carriers present in the active layer of a *M-I-M*-type diode with a hole-injecting and electron-injecting contact at the anode and cathode, respectively, is illustrated in (a). (b) Schematic picture illustrating extraction of the holes using a linearly increasing voltage pulse; for a large A, the whole charge-carrier distribution moves as a uniform package. The red dotted lines show the carrier profile after times t_1 and t_2 have elapsed. In (c), a schematic of the corresponding time-dependent part of the extraction current is shown.

respectively. A schematic picture of the carrier profiles is shown in Fig. 2(a).

Upon applying the reverse-biased linear voltage pulse, the holes are extracted at the anode. The corresponding total current transient $j(t)$ for $0 < t \leq t_{\text{pulse}}$ is given by

$$j(t) = \frac{\varepsilon\varepsilon_0}{d}\frac{\partial V}{\partial t} + \frac{1}{d}\int_0^d J_c(x,t)dx = j_0 + \Delta j(t) \quad (3)$$

where ε is the relative permittivity, $J_c(x,t)$ is the conduction current, $j_0 = -\varepsilon\varepsilon_0 A/d$ is the geometric capacitive response, and $\Delta j(t)$ is the spatially averaged conduction current.

In the limit of $A \to \infty$, the extraction rate is solely governed by drift and an analytical expression for the extraction current can be obtained. Under these conditions, the charge carriers are all extracted with the same velocity. Subsequently, the carrier distribution remains intact during the extraction process, moving uniformly toward the anode contact, leaving a region of thickness $w(t)$ depleted of holes behind in the active layer; see Fig. 2(b). The conduction current within the nondepleted region is

$$\begin{aligned} J_c(x,t) &= e\mu p(x,t)\left[F_0 - \frac{At}{d}\right] - \mu kT\frac{dp(x,t)}{dx} \\ &\approx J_{\text{off}} - ep(x,t)\mu\frac{At}{d}, \end{aligned} \quad (4)$$

where $p(x,t)$ is the charge-carrier density distribution within the semiconductor layer. This distribution of carriers is extracted with a drift velocity $dw/dt = \mu At/d$ with the extraction depth $w(t)$ then given by

$$w(t) = \frac{\mu A t^2}{2d} = \left(\frac{t}{t_{\text{tr}}}\right)^2 d, \quad (5)$$

where $t_{\text{tr}} = \sqrt{2d^2/\mu A}$ corresponds to the time when $w = d$. Concomitantly, the charge-carrier density can be expressed as

$$p(x,t) = \begin{cases} N_1 \exp\left(-\frac{eU}{kT}\left[\frac{x}{d} + \frac{t^2}{t_{\text{tr}}^2}\right]\right), & \text{if } x \leq d - w(t) \\ 0, & \text{if } x > d - w(t) \end{cases} \quad (6)$$

where $p(x,t) = p_0(x + w(t))$ becomes equal to the steady-state carrier density $p_0(x)$ at $t = 0$. Taking the impact of the current passing through the device prior to the pulse to be negligible in this limit, inserting Eq. (4) into Eq. (3), the time-dependent extraction current $\Delta j(t)$ can be readily obtained. Then, with the hole density given by Eq. (6), one finds

$$\begin{aligned} \Delta j(t) &= -\frac{e\mu At}{d^2}\int_0^d p(x,t)dx \\ &= -\frac{kT\mu N_1 At}{Ud}\left[\exp\left(-\frac{eUt^2}{kTt_{\text{tr}}^2}\right) - \exp\left(-\frac{eU}{kT}\right)\right] \end{aligned} \quad (7)$$

for $0 \leq t \leq t_{\text{tr}}$. A schematic picture of the extraction current is shown in Fig. 2(c).

The maximum extraction-current time $t_{\max}$ is obtained after setting the time derivative of the extraction current $\Delta j(t)/j_0$ to zero and evaluating in the $eU \gg kT$ limit, as $t_{\max} = t_{\text{tr}}\sqrt{kT/2eU}$, which is accurate for $eU/kT > 4$ with a less than 2% relative error. Hence, the mobility is related to $t_{\max}$ via

$$\mu = \frac{kT}{e(V_{\text{bi}} - V_{\text{off}})}\frac{d^2}{At_{\max}^2} \quad (8)$$

for $V_{\text{off}} < V_{\text{bi}} - 4kT/e$. Equation (8) predicts a linear dependence between $t_{\max}^{-2}$ and V_{off}:

$$t_{\max}^{-2} = \frac{eA\mu}{kTd^2}(V_{\text{bi}} - V_{\text{off}}). \quad (9)$$

Subsequently, upon plotting $t_{\max}^{-2}$ as a function of V_{off} (keeping the other parameters fixed), an approximation of V_{bi} is

directly obtained from the intersection with the V_{off}-axis of the extrapolated line. The above analysis assumes the transport to be hole(electron)-dominated, where μ corresponds to the hole(electron) mobility $\mu_p(\mu_n)$. By repeating the derivation for the case with two carrier types and considering recombination to be negligible, it can easily be verified that the same final result, Eq. (8), is also obtained for the case with symmetric carrier profiles [Fig. 2(a)] when the mobilities are equal ($\mu = \mu_p = \mu_n$).

It should be noted that in the derivation of Eq. (8), space-charge effects are assumed to be negligible. In the case of Ohmic injecting contacts, however, a significant energy-level bending may be present in the vicinity of the contact. This leads to an effectively reduced built-in voltage inside the active layer [13]. The V_{bi} in Eq. (8) should, in this case, be considered an effective built-in voltage.

In the above derivation, it is also assumed that the active layer is undoped and trap-free. However, it has been previously suggested in the literature that the charge transport in organic semiconductors is dominated by a trapping and release process. For example, Hanfland *et al*. have suggested that the charge carrier mobility is highly charge-density dependent due to the presence of a large number of trap states [9]. If this is the case, then the carrier mobility will not necessarily be constant for varying offset voltages, which means that Eqs. (8) and (9) will no longer be valid. We note, however, that the effect of traps on the charge transport and recombination in organic semiconductors is a debated matter in literature, for example, Tvingstedt and Deibel [14] found that trap states do not dominate the behavior of several commonly used organic solar cell materials. The influence of traps on the measurement method presented in this work is discussed in the results and discussion section.

III. RESULTS AND DISCUSSION

A. Numerical simulations

To validate the analytical derivation, numerical simulations based on a one-dimensional drift-diffusion model [15,16] are carried out. An injection barrier of 0.20 eV for holes and electrons is assumed at the respective injecting contacts and the built-in voltage is set to $V_{\text{bi}} = 0.80$ V; cf. Fig. 1(c). The default parameters used in the simulations are $d = 200$ nm, $\mu_p = 10^{-4}$ cm^2/V s, and $A = 10^6$ V/s. The bulk recombination is assumed to be bimolecular and of the Langevin type (see [15,16]). We note, however, that since the carriers are mainly concentrated at their respective contacts, the recombination is negligible for voltages below V_{bi}.

In Fig. 3(a), the mobilities extracted from simulated current transients are shown for different offset voltages for the case with hole-dominated ($\mu_p \gg \mu_n$) and balanced-current transport ($\mu_p = \mu_n$). It can be seen that when using the standard CELIV equation for mobility determination,

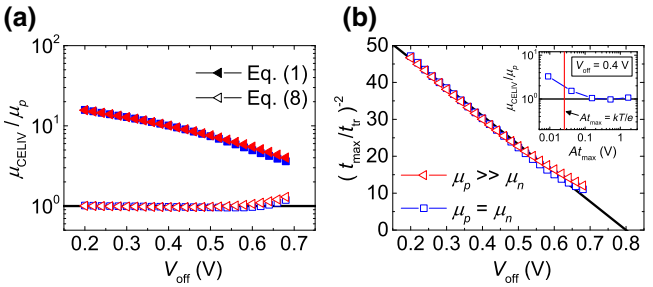

FIG. 3. In (a), the simulated CELIV mobility μ_{CELIV}, relative to the input mobility μ of the faster carrier, is plotted as a function of the applied offset voltage V_{off} for $\mu_p \gg \mu_n$ (red triangles) and $\mu_p = \mu_n$ (blue squares). The filled symbols correspond to mobilities calculated using the standard CELIV theory given by Eq. (1). The open symbols show the extracted mobilities after correcting for the carrier profile, Eq. (8). In (b), the corresponding simulated t_{max} values are plotted as $(t_{\text{max}}/t_{\text{tr}})^{-2}$ as a function of V_{off}, where $t_{\text{tr}}^2 \equiv 2d^2/\mu A$. The offset-voltage dependence predicted by Eq. (9) is depicted by the black solid line. In the inset: the simulated CELIV mobilities, obtained by Eq. (8) as a function of At_{max}, are simulated.

Eq. (1), the mobility is overestimated by over an order of magnitude depending on the applied V_{off}. In contrast, when using Eq. (8) to extract the mobility in Fig. 3(a), an excellent agreement is obtained for the considered voltage range. Equation (8) explains the apparent offset voltage dependence of the mobility obtained when using Eq. (1). In other words, not accounting for the nonuniform carrier distribution leads to an overestimation of the mobility by a factor of approximately $2e(V_{\text{bi}} - V_{\text{off}})/3kT$. For $V_{\text{bi}} - V_{\text{off}} = 0.4$ V, Eq. (1) overestimates the mobility by a factor of 10. This also explains the deviation obtained by Hanfland *et al*. in the limit of negligible trapping (i.e., trap depths smaller than kT/e, when the transport is essentially trap-free) [9].

The corresponding t_{max} values, plotted as $(t_{\text{max}}/t_{\text{tr}})^{-2}$ for different offset voltages V_{off}, are simulated in Fig. 3(b). Indeed, as expected from Eq. (9) (indicated by the black solid line), the simulated $(t_{\text{max}}/t_{\text{tr}})^{-2}$ exhibits a linear dependence with the applied offset voltage. It should be stressed that the above derivation [Eqs. (8) and (9)] assumes the applied transient electric field is large enough for the current transient to be dominated by drift. In the inset of Fig. 3(b), the simulated CELIV mobility, as obtained by Eq. (8), is shown for varying At_{max}. It can be seen that, in practice, the condition for drift-dominated transport is valid when $At_{\text{max}} \gg kT/e$.

It is important to note that the RC time constant, determined by the resistance of the external circuit R and the geometric capacitance of the device C, becomes increasingly important in this kind of CELIV measurement where the extracted charge carriers are situated close to the contact. The RC time can restrict the magnitude of the voltage slope A that can be applied in the measurement. The impact

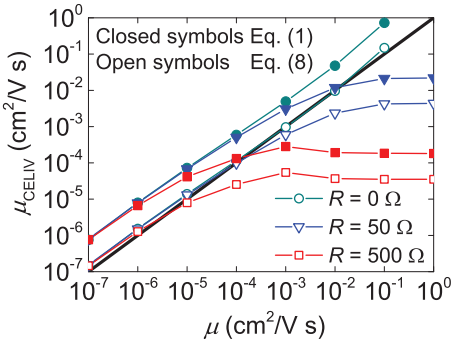

FIG. 4. The effect of the RC time constant on the mobility determination. The simulated CELIV mobility, as extracted using Eq. (1) (filled symbols) or Eq. (8) (open symbols), is shown as a function of the input mobility at $V_{\text{off}} = 0.6$ V. Here, the resistances $R = 50\ \Omega$ and $R = 500\ \Omega$ correspond to RC time constants of $RC = 0.027\ \mu$s and $RC = 0.27\ \mu$s, respectively. A hole-only device having a device area of 4 mm^2 is assumed. The black solid line indicates the input mobility.

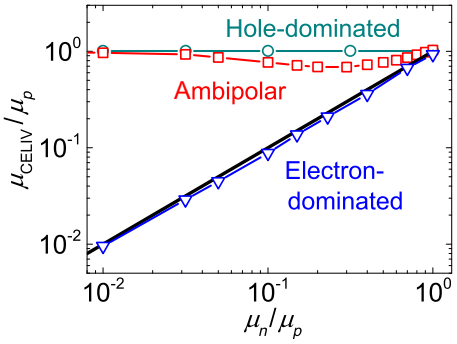

FIG. 5. The CELIV mobilities μ_{CELIV}, extracted using Eq. (8), are simulated as a function of electron mobility μ_n for different devices. The ambipolar device (squares) corresponds to the case when the electron density at the cathode is equal to the hole density at the anode; cf. Fig. 2(a). The device is made electron-dominated (triangles) by increasing the hole injection barrier at the anode (from 0.2 to 0.4 eV), significantly reducing the number of holes within the active layer. Similarly, the hole-dominated device (circles) is obtained by increasing the electron injection barrier at the cathode. The solid black line depicts the input electron mobility.

of the RC time constant has been evaluated for different mobilities in Fig. 4, where the mobility as determined by CELIV is plotted as a function of the actual input mobility. Again, the standard CELIV theory Eq. (1) is roughly an order of magnitude off the actual value for low mobilities or for low RC times. The mobility is restricted by the RC time constant when $t_{\text{max}} \sim 5RC$. We note that the effect of RC on the mobility determination can, for a first approximation, be corrected for by replacing t_{max} with $(t_{\text{max}} - 3RC)$ in Eq. (8) (for $t_{\text{max}} > 5RC$).

For the ambipolar device considered in Fig. 3, because it has equal numbers of electrons and holes within the active layer, the extracted mobility is given by the faster carrier for the case with highly imbalanced mobilities. In Fig. 5, the extracted mobilities using Eq. (8) are simulated for varying μ_n/μ_p. For the ambipolar device, it can be seen that when the electron and hole mobilities are of the same magnitude, the extracted mobility is roughly given by their arithmetic mean $\mu_{\text{CELIV}} \approx (\mu_p + \mu_n)/2$. As μ_n/μ_p is reduced, in turn, the extracted mobility eventually approaches the mobility μ_p of the faster carrier (in this case holes). However, by increasing the injection barrier at the hole-injecting contact, the average hole density can be significantly reduced. At large hole-injection barriers, the device becomes electron-dominated, allowing for the electron mobility to be extracted using Eq. (8), as shown in Fig. 5. Similarly, by increasing the electron-injection barrier at the electron contact (hole-dominated device), the interference from the electrons can be completely removed and hole mobility obtained. In the general case, the carrier type that is more conductive during the extraction process will dominate the current transient, where the conductivity is determined by mobility times the average charge density of the extracted carriers.

Based on the extended theory, as demonstrated in Fig. 5, dark CELIV can now be used to separately determine the electron and hole mobilities by changing the energetics at the injecting contacts. This has previously only been possible using a metal-insulator-semiconductor structure (*M-I-S* CELIV), where a large offset voltage is used to create a charge reservoir against a blocking insulator layer [17,18]. However, the mobility determination with *M-I-S* CELIV has been found to be strongly dependent on the injecting contact [19], and requires good blocking layers [20]. Since the extended CELIV (with a small offset voltage) does not require blocking layers and the injecting contact is automatically taken into account, this method does not suffer from the same limitations.

B. Experimental demonstration

The extended CELIV method has been experimentally tested on polymer-fullerene bulk-heterojunction solar cells with *M-I-M* device structures ITO/PEDOT:PSS/P3HT:PCBM/LiF/Al and ITO/P3HT:PCBM/LiF/Al, with an active layer consisting of a blend of poly(3-hexylthiophene-2,5-diyl) (P3HT) and [6,6]-phenyl C61 butyric acid methyl ester (PCBM) in a 1:1 weight ratio and with a hole transport layer consisting of Poly(2,3-dihydrothieno-1,4-dioxin)-poly(styrenesulfonate) (PEDOT:PSS). See the Supplemental Material [21] for the experimental information and for the IV curves of the solar cells. Measured CELIV current transients, where V_{off} is varied, are shown in Fig. 6(a) for a device with a PEDOT:PSS interlayer. The built-in potential is determined in Fig. 6(b) where t_{max}^{-2} is plotted as a function of V_{off} for a device both with and

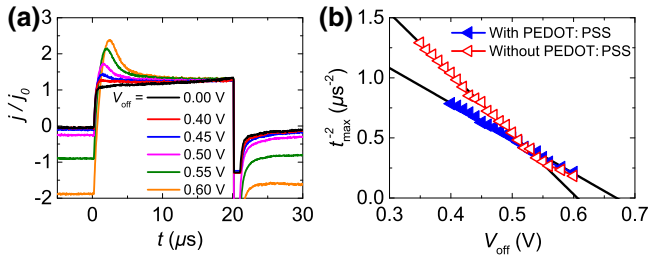

FIG. 6. (a) CELIV transients of an ITO/PEDOT:PSS/P3HT:PCBM/LiF/Al solar cell for $A = 2$ V/20 μs plotted for different offset voltages V_{off}, between 0 and 0.6 V. (b) The corresponding extracted t_{max}^{-2} as a function of V_{off} is shown; V_{bi} is determined from the intersection with the V_{off}-axis of a linear fit to the plot. A device without the PEDOT:PSS interlayer has been included for comparison.

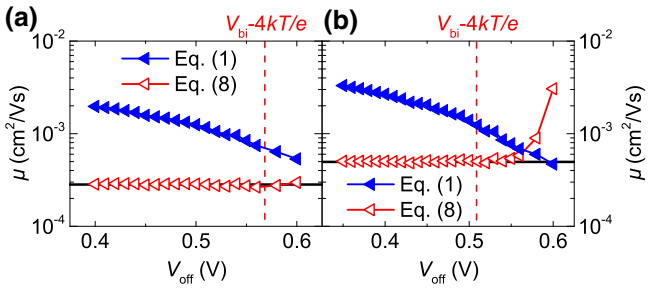

FIG. 7. The experimental CELIV mobilities for different values of V_{off} are shown for the P3HT:PCBM device (a) with a PEDOT:PSS interlayer and (b) without a PEDOT:PSS layer. The closed symbols correspond to mobilities obtained by the standard uniform profile approximation [Eq. (1)], whereas mobilities corrected for the injected carrier profile [Eq. (8)] are indicated by the open symbols.

without a PEDOT:PSS interlayer. By using a linear fit to the lower V_{off} values in Fig. 6(b), as per Eq. (9), we get $V_{bi} = 0.67$ V and $V_{bi} = 0.61$ V for the device with and without a PEDOT:PSS layer, respectively. The value for the device with a PEDOT:PSS layer is in good agreement with the results of Mingebach *et al.* [22]. The measured decrease in V_{bi} upon removing the PEDOT:PSS layer, seen in Fig. 6(b), indicates that the work function of the anode decreases, as expected. The decrease in work function also decreases the density of holes diffusing into the active layer from the anode. We note that the built-in potential is often not directly determined from the work function difference of the contacts, e.g., energy-level bending (or Fermi-level pinning) might cause the built-in potential to be smaller than the work-function difference [13]. Therefore, a change of only 0.06 V is reasonable when leaving out the PEDOT:PSS layer. Additionally, the work function of ITO is known to change with processing conditions and is, therefore, not well defined [23].

It is important to check that the extracted t_{max} values follow a linear behavior in the correct offset-voltage regime in the plot in Fig. 6(b). We assume an undoped and trap-free active layer with a constant mobility in the theory and analysis presented here. If the active layer is doped, the *M-I-M* picture is no longer valid and the analysis fails. Doping can be seen as a large extraction current, $\Delta j \gg j_0$, in the CELIV transients [6], meaning that the semiconductor can no longer be considered as an insulator, which is clearly not the case in the measured transients in Fig. 6(a). The effect of trapping has been evaluated in the Supplemental Material [21]. It is seen that the extracted built-in potential is influenced by local energy-level bending at the contacts; at large trap densities, V_{bi} might be strongly overestimated due to this bending. The extracted mobility reflects an effective mobility

$$\mu_{eff} = \mu_{free} \times \frac{p_{free}}{p_{free} + p_{trap}}, \tag{10}$$

where μ_{free} is the band mobility of free carriers, p_{free} is the density of free carriers, and p_{trap} is the density of trapped carriers. At low trap densities, the effective mobility approaches the free-carrier mobility. This method measures the effective mobility of charges extracted at a distance of approximately $x \sim dkT/q[V_{bi} - V_{off}]$ from the contact.

Since the extracted V_{bi} in the presented experimental data corresponds well to the expected value [22], it is reasonable to assume that trapping has a negligible effect on the experimental data. This is further supported by previous measurements conducted in the same laboratory; using photoinduced absorption, the trap depth was determined to 21.3 ± 0.3 meV [24], meaning essentially no trapping at room temperature.

From the slope in Fig. 6(b), a mobility of $\mu = 2.8 \times 10^{-4}$ cm^2/V s is found for the device with a PEDOT:PSS layer and $\mu = 5.0 \times 10^{-4}$ cm^2/V s is found for the device without the interlayer. The extracted mobility for each transient is plotted in Fig. 7 as a function of V_{off}. For higher V_{off}, close to V_{bi}, Eq. (8) is no longer valid as the magnitude, and the associated space-charge effects of the injected current become significant; this is seen as a deviation from the linear fit in Fig. 6(b) and as an error in the mobility estimation in Fig. 7(b). For these devices, the mobility measurements are restricted to a narrow offset-voltage range of about 0.15 V; keeping V_{off} lower than V_{bi} but high enough for accurate determination of t_{max}.

Earlier studies have shown that electrons are the faster charge carrier in blends of P3HT:PCBM [25,26], which should result in electrons having a higher conductivity and dominating the current transient in the case of equally large concentrations of holes and electrons in the active layer. The increase in mobility observed here without the PEDOT:PSS layer, see Fig. 7, agrees with a decrease in the hole density (due to the decreased anode work function) resulting in the faster electrons now dominating the

extraction-current transient. This also implies that electrons are clearly not dominating the current transient in the device with a PEDOT:PSS interlayer, meaning that the ITO/PEDOT:PSS anode injects a larger density of holes into the active layer than the density of electrons injected by the LiF/Al cathode. Generally, the LiF/Al cathode is very sensitive to thickness optimization of the LiF layer and the low work-function contact is also prone to degradation, which might be the reason for the lower conductivity of electrons in our measurements [27]. The measured mobility in both cases, with and without a PEDOT:PSS interlayer, might still be influenced by both electrons and holes, which means that a larger barrier at the anode or a more Ohmic contact than the LiF/Al cathode might be needed for measuring the pure electron mobility or vice versa for measuring the pure hole mobility.

IV. CONCLUSIONS

We extend the dark CELIV method for simultaneous determination of the built-in potential and the equilibrium carrier mobility in thin-film *M-I-M* diodes with injecting contacts. The same theory is also applicable to the *p-i-n* device structure with an intrinsic semiconductor layer sandwiched between highly doped *p*- and *n*-type semiconductor layers. The extended method is demonstrated through drift-diffusion simulations and experimentally on organic solar cells. It follows from the simulations and the experimental results that careful tuning of the contact properties enables hole and electron mobilities to be selectively measured. The simplicity of the method, a rather quick measurement with modest equipment requirements, will make it very useful for future in-device characterization of the built-in potential and mobility in thin-film solar cells of *M-I-M* and *p-i-n* types.

ACKNOWLEDGMENTS

Partial financial support from the Academy of Finland through Project No. 279055 and the Jane and Aatos Erkko foundation through project ASPIRE is acknowledged. S.D. acknowledges funding from the Otto A. Malm foundation and the Vilho, Yrjö and Kalle Väisälä Foundation. O.J.S. acknowledges funding from the Swedish Cultural Foundation in Finland.

S.D. and O.J.S. contributed equally to this work.

[1] G. Juška, K. Arlauskas, M. Viliūnas, and J. Kočka, Extraction Current Transients: New Method of Study of Charge Transport in Microcrystalline Silicon, Phys. Rev. Lett. **84**, 4946 (2000).

[2] G. Juška, K. Arlauskas, M. Viliūnas, K. Genevičius, R. Österbacka, and H. Stubb, Charge transport in π-conjugated polymers from extraction current transients, Phys. Rev. B **62**, R16235 (2000).

[3] C. Deibel, Charge carrier dissociation and recombination in polymer solar cells, Phys. Status Solidi A **206**, 2731 (2009).

[4] S. Bange, M. Schubert, and D. Neher, Charge mobility determination by current extraction under linear increasing voltages: Case of nonequilibrium charges and field-dependent mobilities, Phys. Rev. B **81**, 035209 (2010).

[5] J. Lorrmann, B. H. Badada, O. Inganäs, V. Dyakonov, and C. Deibel, Charge carrier extraction by linearly increasing voltage: Analytic framework and ambipolar transients, J. Appl. Phys. **108**, 113705 (2010).

[6] O. J. Sandberg, M. Nyman, and R. Österbacka, Direct determination of doping concentration and built-in voltage from extraction current transients, Org. Electron. **15**, 3413 (2014).

[7] G. Juška, N. Nekrašas, V. Valentinavičius, P. Meredith, and A. Pivrikas, Extraction of photogenerated charge carriers by linearly increasing voltage in the case of Langevin recombination, Phys. Rev. B **84**, 155202 (2011).

[8] M. Nyman, F. Pettersson, and R. Österbacka, Origin of equilibrium charges in poly(3-hexylthiophene):[6,6]-phenyl-C_{61}-butyric acid methyl ester solar cell devices, Chem. Phys. **404**, 60 (2012).

[9] R. Hanfland, M. A. Fisher, W. Brütting, U. Würfel, and R. C. I. MacKenzie, The physical meaning of charge extraction by linearly increasing voltage transients from organic solar cells, Appl. Phys. Lett. **103**, 063904 (2013).

[10] S. L. M. van Mensfoort and R. Coehoorn, Effect of Gaussian disorder on the voltage dependence of the current density in sandwich-type devices based on organic semiconductors, Phys. Rev. B **78**, 085207 (2008).

[11] C. Deibel, A. Wagenpfahl, and V. Dyakonov, Origin of reduced polaron recombination in organic semiconductor devices, Phys. Rev. B **80**, 075203 (2009).

[12] P. Kumar, S. C. Jain, V. Kumar, S. Chand, and R. P. Tandon, A model for the J-V characteristics of P3HT:PCBM solar cells, J. Appl. Phys. **105**, 104507 (2009).

[13] P. de Bruyn, A. H. P. van Rest, G. A. H. Wetzelaer, D. M. de Leeuw, and P. W. M. Blom, Diffusion-Limited Current in Organic Metal-Insulator-Metal Diodes, Phys. Rev. Lett. **111**, 186801 (2013).

[14] K. Tvingstedt and C. Deibel, Temperature dependence of ideality factors in organic solar cells and the relation to radiative efficiency, Adv. Energy Mater. **6**, 1502230 (2016).

[15] O. J. Sandberg, M. Nyman, and R. Österbacka, Effect of Contacts in Organic Bulk Heterojunction Solar Cells, Phys. Rev. Appl. **1**, 024003 (2014).

[16] S. Sandén, O. Sandberg, Q. Xu, J.-H. Smått, G. Juška, M. Lindén, and R. Österbacka, Influence of equilibrium charge reservoir formation on photo generated charge transport in TiO_2/organic devices, Org. Electron. **15**, 3506 (2014).

[17] G. Juška, N. Nekrašas, and K. Genevičius, Investigation of charge carriers transport from extraction current transients of injected charge carriers, J. Non-Cryst. Solids **358**, 748 (2012).

[18] A. Armin, G. Juška, M. Ullah, M. Velusamy, P. L. Burn, P. Meredith, and A. Pivrikas, Balanced carrier mobilities: Not a necessary condition for high-efficiency thin organic solar

cells as determined by MIS-CELIV, Adv. Energy Mater. **4**, 1300954 (2014).

[19] O. J. Sandberg, M. Nyman, S. Dahlström, S. Sandén, B. Törngren, J.-H. Smått, and R. Österbacka, On the validity of MIS-CELIV for mobility determination in organic thin-film devices, Appl. Phys. Lett. **110**, 153504 (2017).

[20] O. J. Sandberg, S. Sandén, A. Sundqvist, J.-H. Smått, and R. Österbacka, Determination of Surface Recombination Velocities at Contacts in Organic Semiconductor Devices Using Injected Carrier Reservoirs, Phys. Rev. Lett. **118**, 076601 (2017).

[21] See Supplemental Material at http://link.aps.org/supplemental/10.1103/PhysRevApplied.10.054019 for the experimental information, simulations of the effect of traps, and the measured IV curves of the solar cells.

[22] M. Mingebach, C. Deibel, and V. Dyakonov, Built-in potential and validity of the Mott-Schottky analysis in organic bulk heterojunction solar cells, Phys. Rev. B **84**, 153201 (2011).

[23] Y. Zhou, J. W. Shim, C. Fuentes-Hernandez, A. Sharma, K. A. Knauer, A. J. Giordano, S. R. Marder, and B. Kippelen, Direct correlation between work function of indium-tin-oxide electrodes and solar cell performance influenced by ultraviolet irradiation and air exposure, Phys. Chem. Chem. Phys. **14**, 12014 (2012).

[24] S. Sandén, N. M. Wilson, M. Nyman, and R. Österbacka, Characterization of recombination in P3HT:fullerene blends: Clarifying the influence of interfacial states, Org. Electron. **42**, 131 (2017).

[25] V. D. Mihailetchi, H. Xie, B. de Boer, L. J. A. Koster, and P. W. M. Blom, Charge transport and photocurrent generation in poly(3-hexylthiophene): Methanofullerene bulk-heterojunction solar cells, Adv. Funct. Mater. **16**, 699 (2006).

[26] A. Baumann, J. Lorrmann, C. Deibel, and V. Dyakonov, Bipolar charge transport in poly(3-hexyl thiophene)/methanofullerene blends: A ratio dependent study, Appl. Phys. Lett. **93**, 252104 (2008).

[27] S.-H. Lee, J.-H. Kim, T.-H. Shim, and J.-G. Park, Effect of interface thickness on power conversion efficiency of polymer photovoltaic cells, Electron. Mater. Lett. **5**, 47 (2009).